Hindawi
Mathematical Problems in Engineering
Volume 2022, Article ID 9717413, 11 pages
https://doi.org/10.1155/2022/9717413

Research Article

Joint Design Method of Transmit-Receive for Airborne MIMO Radar Based on Feasible Point Pursuit

Jianchong Huang,[1] Zhihui Li,[1] Xiaobo Li,[1] Chunsheng Liu,[1] Chaoyang Niu,[1] Xiaoxing Feng,[1] and Qiang Wang[2]

[1]*College of Electronic Engineering, National University of Defense Technology, Hefei 230037, China*
[2]*College of Information and Communication, National University of Defense Technology, Wuhan, China*

Correspondence should be addressed to Zhihui Li; lizhihui_16@163.com

Received 29 March 2022; Accepted 25 May 2022; Published 13 June 2022

Academic Editor: Wang Zheng

Consider the moving target detection performance degradation of airborne multiple-input multiple-output (MIMO) radar in the presence of inaccurate target prior information. This paper proposes a joint design method of transmit waveform and receive filter bank of airborne MIMO radar based on feasible point pursuit successive convex approximation (FPP-SCA). Firstly, a set of receive filter banks is designed in the region where the target may appear on the angle-Doppler plane, and the worst-case output signal-to-clutter-plus-noise ratio (SCNR) is maximized as the optimization criterion. Secondly, considering the energy constraint and similarity on the transmit waveform, the maximin joint design problem is formulated to improve the robustness of the MIMO space-time adaptive processing (STAP) radar against the uncertainty of target parameters. Finally, an FPP-SCA algorithm is employed to solve the maximin nonconvex joint design problem. Simulation results demonstrate the effectiveness of the proposed method in terms of better output SCNR, lower computational load, and more robustness against the errors of target parameters.

1. Introduction

As the information hub of the modern battlefield environment, early warning aircraft can effectively improve the combat effectiveness of the battlefield. As the core of early warning aircraft, airborne radar can expand the detection range of radar to ground, ocean, and air targets [1]. However, the airborne radar suffers from intense ground/sea clutter due to its down-looking mode. The clutter is strongly coupled in the space-time domains, which leads to the weak target signal completely submerged by the clutter and makes it more difficult for airborne radar to detect the moving target [2]. Collecting the received data of the space-time domain, space-time adaptive processing (STAP) can effectively suppress side-lobe clutter and main-lobe clutter and improve the detection performance of moving targets under clutter background [3]. Nevertheless, the airborne radar is faced with threats such as low observable targets, low-altitude target, and advanced integrated electronic jamming in the contemporary battlefield environment. It is necessary to develop new system airborne radar and corresponding new theory and technology of signal processing [4].

Multiple-input multiple-output (MIMO) radar can flexibly transmit different waveforms through different antennas [5]. Utilizing the property of waveform diversity, MIMO radar can design different transmit waveform, which makes it superior to traditional-phased array radar in target detection, parameter estimation, recognition, and classification [6–10]. In addition, making full use the information of the target and environment, the cognitive radar extends the adaptive technology from the receiver to the transmitter [11]. Thus, the cognitive radar forms a fully adaptive radar processing system with a dynamic closed-loop receiver, transmitter, and environment. According to the prior information of the dynamic environment database and the environment information obtained by the radar in real time, cognitive radar can infer and decide the optimal waveform or the waveform parameters suitable for the current radar

working scene. By adaptively adjusting and optimizing the resource allocation of the radar system and the transmit waveform, cognitive radar can obtain the optimal target detection performance in the complex and changeable environment. Inspired by the cognitive idea and MIMO radar, and based on the actual prior environment information, it is possible for the airborne MIMO radar to jointly design the transmit waveform and receive filter to realize the best matching between the system and the environment and improve the target detection performance in the complex environment.

In the past decades, joint design of transmit waveform and receive filter for airborne collocated MIMO radar system has received considerable attention. These research studies can be divided into two categories. The first category deals with the joint design of transmit-receive exploiting the accurate prior information [12–19]. In [12], maximizing the output signal-to-interference-plus-noise ratio (SINR) under the practical waveform constraints (i.e., the energy constraint, constant-envelope constraint, and similarity constraint), the joint design problem is formulated in an earlier time and five iterative algorithms based on generalized Rayleigh quotient, relaxation and waveform extracting, and fractional programming are proposed. In 2016, Setlur and Rangaswamy of the US Air Force Research Laboratory studied the waveform design problem in STAP, which assumed that the clutter response was related to the transmit waveform [13]. Since the objective function of the weight vector and waveform vector is joint nonconvex, while the objective function of a single weight vector and waveform is convex, the constrained selection minimization technology is proposed to iteratively optimize another vector while keeping one vector unchanged. O'Rourke Sean et al. [14] studied the joint design problem of transmit signal and receive beamformer under the signal-dependent STAP, and proposed a relaxed biquadratic optimization method to find a feasible solution. In addition, they extended the energy constraint on waveform to constant-modulus and similarity constraint [15]. In [16], the minorization-maximization (MM) technique is employed to solve the resultant quartic waveform optimization problem. Compared with the semidefinite programming (SDP) method, the joint design algorithm based on MM technique exhibits faster convergence speed and better SINR performance. In [17, 18], the Riemannian geometry optimization method is first applied to the joint design of MIMO-STAP radar, and the Riemannian gradient descent algorithm and the Riemannian trust region algorithms are proposed to solve the joint design problem.

However, the performance of MIMO-STAP radar is severely degraded when the prior information is inaccurate. Then, the second category addresses the robust joint design of transmit-receive in the presence of prior information uncertainties. In [20], considering the presence of target space-time steering vector mismatch, the worst-case output SINR over the set of the target space-time steering vector is maximized as a figure of merit for the robust joint design. However, the waveform covariance matrix obtained by the relaxation constraint of the target steering vector and the diagonal loading technique is still suboptimal. To solve this problem, Tang Bo et al. [21] used a more general uncertainty set to describe the steering vector error, and then accurately derived the worst target steering vector that minimizes the output SINR. This method abandoned the heuristic diagonal loading method to find the globally optimal waveform covariance matrix which is robust to the target steering vector error. In [22], considering the uncertainty of target Doppler frequency and angle, the joint design of MIMO-STAP radar with peak-to-average power ratio (PAPR) and transmit power constraints is studied. However, this method has high computational complexity, and only three independent interference is considered in the simulation scene. In [23], based on the known target Doppler frequency and spatial angle statistical distribution, the averaged output signal-to-clutter-plus-noise ratio (SCNR) is deduced as the optimization criterion, and four robust joint design methods-based SDP relaxation and fractional programming with power method-like are proposed. In [24], the maximin joint design of transmit waveform and receive filter bank under the energy constraint, flexible modulus constraint, and similarity constraint are considered. In [25], with the prior knowledge of target and clutter statistics, the averaged SINR is formulated as a figure of merit to maximize. Then, an iterative algorithm based on Dinkelbach transformation and alternating direction penalty method (ADPM) is proposed to solve the robust joint design problem.

In this paper, focusing on the joint design problem of transmit waveform and receive filter bank of airborne MIMO radar when the target angle and Doppler parameters are inaccurate, a set of filters that are matched with the target possible region is designed. The worst-case output SCNR is maximized as a figure of merit under the constant-modulus constraint and similarity constraint on the transmit waveform. Then, the joint design problem is formulated by maximizing the worst-case SCNR, and a sequential optimization algorithm based on feasible point pursuit successive convex approximation (FPP-SCA) is developed to solve the resultant problem. Simulation results are provided to demonstrate the performance of the proposed algorithm. The main contributions of the paper are summarized as follows: (1) By employing a set of receive filter tuned over the possible spatial angle and Doppler frequency of target, the objective function of joint design is obtained by maximizing the worst-case output SCNR. (2) A sequential optimization algorithm based on FPP-SCA is derived to solve the robust joint design problem. Specifically, an auxiliary variable is introduced to transform the maximin problem into a minimization problem. Then, the nonconvex constant-modulus constraint is solved by utilizing the SCA method. Thus, the waveform optimization problem can be addressed by using the CVX tool box. (3) Several simulation results indicate that the proposed joint design algorithm performs better than the algorithm based on SDP and randomization method in terms of better output SCNR and lower computational time. In addition, the performance of the proposed joint design method is against the target parameters errors.

The remainder of this paper is organized as follows: In Section 2, the signal model of MIMO-STAP radar is provided. The problem formulation and the robust joint design

problem are discussed in Section 3. The sequential optimization algorithm based on FPP-SCA is presented in Section 4. Simulation results are provided in Section 5 to demonstrate the performance of the proposed algorithm. Finally, conclusions are drawn in Section 6.

2. Signal Model

We consider an airborne collocated MIMO radar system with N_T transmit antennas and N_R receive antennas, as shown in Figure 1. The transmit antenna and receive antenna are uniform linear array (ULA) with interelement spacing being d_T and d_R, respectively. The radar transmits M pulses during a coherent processing interval (CPI) with the pulse repetition frequency (PRF) f_r. The radar platform is flying along the X-axis at velocity V_p. Assuming that $\mathbf{s}_n \in \mathbb{C}^{L\times 1}$ represents the sampled waveform emitted by the nth transmit antenna, then the transmit waveform matrix of the radar system can be expressed as $\mathbf{S} = [\mathbf{s}_1, \mathbf{s}_2, \ldots, \mathbf{s}_{N_T}]^T \in \mathbb{C}^{N_T\times L}$, where L represents the number samples of a pulse and each pulse emits the same waveform.

2.1. Target. Assuming that the spatial angle of the moving target relative to the platform is ϕ_t and the normalized Doppler frequency is f_t, then the target echo of the mth pulse received by the airborne MIMO radar can be expressed as

$$\mathbf{y}_{t,m} = \alpha_t e^{j2\pi(m-1)f_t}\left(\mathbf{I}_L \otimes \left(\mathbf{b}(\phi_t)\mathbf{a}^T(\phi_t)\right)\right)\mathbf{s}, \tag{1}$$

where α_t represents the target complex amplitude, $\mathbf{I}_L$ is the $L \times L$ identity matrix, $\otimes$ is the Kronecker product, $(\cdot)^T$ stands for the transpose operation, $\mathbf{s} = \mathrm{vec}(\mathbf{S})$, $\mathbf{a}(\phi_t)$ and $\mathbf{b}(\phi_t)$ represent the transmit spatial steering vector and receive steering vector of target, respectively, and they have the form of

$$\mathbf{a}(\phi_t) = \left[1, e^{\left(j2\pi d_T \cos(\phi_t)/\lambda\right)}, \ldots, e^{\left(j2\pi(N_T-1)d_T\cos(\phi_t)/\lambda\right)}\right]^T, \tag{2}$$

$$\mathbf{b}(\phi_t) = \left[1, e^{\left(j2\pi d_R \cos(\phi_t)/\lambda\right)}, \ldots, e^{\left(j2\pi(N_R-1)d_R\cos(\phi_t)/\lambda\right)}\right]^T, \tag{3}$$

where λ denotes the wavelength of the system.

Let $\mathbf{y}_t = [\mathbf{y}_{t,1}^T, \ldots, \mathbf{y}_{t,M}^T]^T \in \mathbb{C}^{LMN_R\times 1}$, then the received target echo of a CPI can be expressed as

$$\mathbf{y}_t = \alpha_t \mathbf{V}(f_t, \phi_t)\mathbf{s}, \tag{4}$$

where $\mathbf{V}(f_t, \phi_t) = (\mathbf{u}(f_t) \otimes \mathbf{I}_L \otimes (\mathbf{b}(\phi_t)\mathbf{a}^T(\phi_t)))$, and $\mathbf{u}(f_t) = [1, e^{j2\pi f_t}, \ldots, e^{j2\pi(M-1)f_t}]^T$ represents the time steering vector of target.

2.2. Clutter. The clutter of airborne MIMO radar system is the signal-dependent clutter echo, which is distributed in the whole azimuth domain and range domain. Clutter echo received by a single range bin consists of all clutter patches of

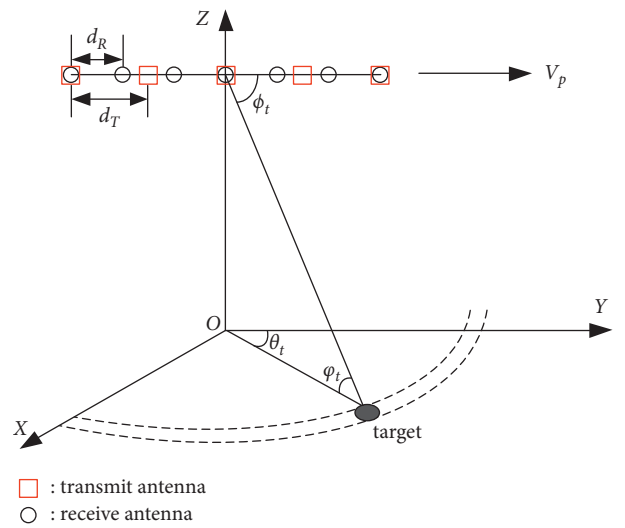

Figure 1: Configuration of airborne MIMO radar.

the range bin. Then, the clutter echo received by the airborne MIMO radar can be expressed as

$$\mathbf{y}_c = \sum_{p=-P}^{P}\sum_{k=1}^{N_c} \alpha_{c,p,k}\mathbf{V}\left(f_{c,p,k}, \phi_{c,p,k}\right)\mathbf{s}, \tag{5}$$

Where P denotes the number of range bin around the range under test, $\alpha_{c,p,k}$, $f_{c,p,k}$, and $\phi_{c,p,k}$ represent the complex amplitude, normalized Doppler frequency, and spatial angle of the kth clutter patch in the pth range bin, respectively, $f_{c,p,k} = 2V_p\cos(\phi_{c,p,k})/(\lambda f_r)$, N_c is the clutter patch number in a range bin. $\mathbf{V}(f_{c,p,k}, \phi_{c,p,k}) = (\mathbf{u}(f_{c,p,k}) \otimes \mathbf{J}_P^T \otimes (\mathbf{b}(\phi_{c,p,k})\mathbf{a}^T(\phi_{c,p,k})))$, let $\mathbf{V}_{c,p,k}$ denote $\mathbf{V}(f_{c,p,k}, \phi_{c,p,k})$ for convenience, where $\mathbf{J}_p = \mathbf{J}_{-p}^T \in \mathbb{C}^{L\times L}$ denotes the shift matrix, which is calculated by

$$\mathbf{J}_p(i,j) = \begin{cases} 1, & i-j+p=0, \\ 0, & i-j+p\neq 0. \end{cases} \tag{6}$$

Total received echo: therefore, the echo received by the airborne radar containing the target (which may exist), signal-dependent clutter, and noise can be expressed as

$$\mathbf{y} = \mathbf{y}_t + \mathbf{y}_c + \mathbf{y}_n, \tag{7}$$

where $\mathbf{y}_n$ denotes the complex Gaussian white noise whose mean value is zero and covariance matrix is $\sigma_n^2\mathbf{I}_{LMN_R}$, where σ_n^2 is noise power.

3. Problem Formulation

Considering that the accurate normalized Doppler frequency and spatial angle of the target are unknown, it is assumed that the approximate region of the target in the angle-Doppler plane can be known through spatial angle estimation and Doppler frequency estimation, as shown in cyan area in Figure 2. The normalized Doppler frequency and spatial angle range of the target can be expressed as $\Psi = [f_{tmin}, f_{tmax}]\,(f_t \in \Psi)$ and $\Omega = [\phi_{tmin}, \phi_{tmax}]\,(\phi_t \in \Omega)$, respectively, and are then discretized into I and J grid points,

respectively. Then, we can obtain the discretized normalized Doppler frequency-spatial angle pair, that is, $(f_t^{n_1}, \phi_t^{n_2}), n_1 \in \mathscr{I} = \{1, \ldots, I\}, n_2 \in \mathscr{J} = \{1, \ldots, J\}$. Next, a set of $LMN_R \times 1$ filters $\mathbf{w}_{n_1,n_2} \in \mathscr{W} = \left\{\mathbf{w}_{n_1,n_2} | n_1 \in \mathscr{I}, n_2 \in \mathscr{J}\right\}$ is used to process the received signal, and each received filter is tuned to a specific normalized Doppler frequency-spatial angle pair of targets $(f_t^{n_1}, \theta_t^{n_2})$. Therefore, the output SCNR corresponding to the (n_1, n_2) th filter branch can be expressed as

$$\mathrm{SCNR}_{n_1,n_2}\left(\mathbf{s}, \mathbf{w}_{n_1,n_2}\right) = \frac{\sigma_t^2 \left|\mathbf{w}_{n_1,n_2}^H \mathbf{V}\left(f_t^{n_1}, \phi_t^{n_2}\right)\mathbf{s}\right|^2}{\mathbf{w}_{n_1,n_2}^H \mathbf{R}_{\mathrm{cn}}(\mathbf{s}) \mathbf{w}_{n_1,n_2}}, \tag{8}$$

where $\sigma_t^2 = \mathbb{E}\left\{|\alpha_t|^2\right\}$, $\mathbb{E}(\cdot)$ denotes the statistical expectation, $(\cdot)^H$ denotes the conjugate transpose operation, $\mathbf{R}_{\mathrm{cn}}(\mathbf{s})$ is the clutter plus noise covariance matrix, which can be expressed as

$$\mathbf{R}_{\mathrm{cn}}(\mathbf{s}) = \sum_{p=-P}^{P} \sum_{k=1}^{N_c} \sigma_{c,p,k}^2 \mathbf{V}_{c,p,k} \mathbf{s}\mathbf{s}^H \mathbf{V}_{c,p,k}^H + \sigma_n^2 \mathbf{I}_{LMN_R}. \tag{9}$$

Assumed that the prior information of clutter (including $\sigma_{c,p,k}^2$, $f_{c,p,k}$ and $\phi_{c,p,k}$) is known, which can be obtained from the terrain database. Therefore, maximizing the worst-case output SCNR over all possible normalized Doppler frequencies and spatial angles of the target, we can obtain the optimization of the joint design to deal with the uncertainty of the target parameters. Concretely, the joint design of transmit waveform and receive filter bank for airborne MIMO radar in the presence of target uncertainty can be formulated as

$$\overline{\mathrm{SCNR}}\left(\mathbf{s}, \mathbf{w}_{n_1,n_2}\right) \triangleq \min_{n_1 \in \mathscr{I}, n_2 \in \mathscr{J}} \mathrm{SCNR}_{n_1,n_2}\left(\mathbf{s}, \mathbf{w}_{n_1,n_2}\right). \tag{10}$$

In practical radar system, constant-modulus constraint is applied to the transmit waveform to prevent overloading of the amplifier, i.e., $|\mathbf{s}(n)| = 1/\sqrt{N_T L}$, $n = 1, \ldots, N_T L$. At the same time, in order to obtain the good characteristics for the transmit waveform, for example, good ambiguity function, it is necessary to impose similarity constraints on the transmit waveform, namely, $\|\mathbf{s} - \mathbf{s}_0\|_\infty \le \delta$, where, $\|\cdot\|_\infty$ represents the infinite norm of a matrix, δ is used to control the similarity between the optimized waveform and the reference waveform $\mathbf{s}_0$ ($\|\mathbf{s}_0\|^2 = 1$), and $\|\cdot\|$ represents the Euclidean norm of a matrix.

Considering the constant-modulus constraint and similarity constraint of the transmit waveform, the joint design problem of transmit waveform and receive filter bank of airborne MIMO radar based on maximizing the worst-case output SCNR can be expressed as

$$\begin{aligned} &\max_{\mathbf{s}, \mathbf{w}_{n_1,n_2} \in \mathscr{W}} \mathrm{SCNR}_{n_1,n_2}\left(\mathbf{s}, \mathbf{w}_{n_1,n_2}\right), \\ &|\mathbf{s}(n)| = \frac{1}{\sqrt{N_T L}}, \quad n = 1, \ldots, N_T L, \\ &\text{s.t.} \\ &\left\|\mathbf{s} - \mathbf{s}_0\right\|_\infty \le \delta, \end{aligned} \tag{11}$$

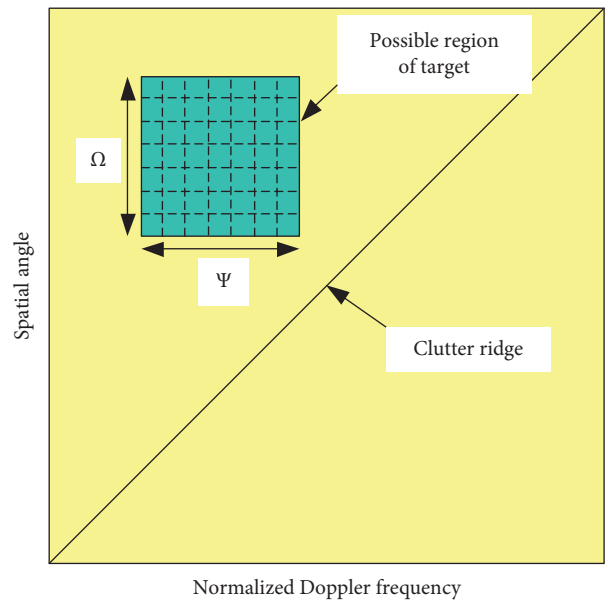

Figure 2: Possible region of target in angle-doppler plane.

The problem (11) is NP hard owing to the nonconvex objective function and the nonconvex waveform constraints. In the next section, we proposed a sequential algorithm to address the problem (11).

4. Joint Design Method Based on FFP-SCA

In this section, a sequential algorithm based on FPP-SCA is proposed to solve the maximin problem (11), which can obtain monotonically increasing worst-case output SCNR during the iterative procedure. Specifically, the transmit waveform $\mathbf{s}$ is first fixed, and the receive filter banks $\mathbf{w}_{n_1,n_2} \in \mathscr{W}$ are optimized by maximizing $\overline{\mathrm{SCNR}}(\mathbf{s}, \mathbf{w}_{n_1,n_2})$. Then, the receive filter banks $\mathbf{w}_{n_1,n_2} \in \mathscr{W}$ are fixed and the transmit waveform $\mathbf{s}$ is optimized.

4.1. Receive Filter Bank Optimization. At the ith iteration, the optimization of the receive filter bank $\mathbf{w}_{n_1,n_2} \in \mathscr{W}$ can be expressed as

$$\max_{\mathbf{w}_{n_1,n_2} \in \mathscr{W}} \frac{\left|\mathbf{w}_{n_1,n_2}^H \mathbf{V}\left(f_t^{n_1}, \phi_t^{n_2}\right)\mathbf{s}^{(i-1)}\right|^2}{\mathbf{w}_{n_1,n_2}^H \mathbf{R}_{\mathrm{cn}}\left(\mathbf{s}^{(i-1)}\right)\mathbf{w}_{n_1,n_2}}. \tag{12}$$

The optimization problem (12) has IJ independent objective functions corresponding to $\mathbf{w}_{n_1,n_2}$. Therefore, the problem (12) can be transformed into optimization of each $\mathbf{w}_{n_1,n_2}$, and the closed solution of $\mathbf{w}_{n_1,n_2}$ can be obtained by

$$\mathbf{w}_{n_1,n_2}^{(i)} = \frac{\mathbf{R}_{\mathrm{cn}}^{-1}\left(\mathbf{s}^{(i-1)}\right)\mathbf{V}\left(f_t^{n_1}, \theta_t^{n_2}\right)\mathbf{s}^{(i-1)}}{\left(\mathbf{s}^{(i-1)}\right)^H \mathbf{V}^H\left(f_t^{n_1}, \theta_t^{n_2}\right)\mathbf{R}_{\mathrm{cn}}^{-1}\left(\mathbf{s}^{(i-1)}\right)\mathbf{V}\left(f_t^{n_1}, \theta_t^{n_2}\right)\mathbf{s}^{(i-1)}}. \tag{13}$$

4.2. Transmit Waveform Optimization Based on FPP-SCA. With a fixed receive filter bank $\mathbf{w}_{n_1,n_2}$, the optimization of the transmit waveform $\mathbf{s}$ can be expressed as

$$\begin{aligned}&\max_{\mathbf{s}} \min_{n_1\in\mathcal{F},n_2\in\mathcal{J}} \frac{\left|\left(\mathbf{w}_{n_1,n_2}^{(i)}\right)^H \mathbf{V}\left(f_t^{n_1},\phi_t^{n_2}\right)\mathbf{s}\right|^2}{\left(\mathbf{w}_{n_1,n_2}^{(i)}\right)^H \mathbf{R}_{\mathrm{cn}}\left(\mathbf{s}^{(i-1)}\right)\mathbf{w}_{n_1,n_2}^{(i)}},\\ &\text{s.t.}\quad |\mathbf{s}(n)| = \frac{1}{\sqrt{N_T L}},\quad n=1,\cdots,N_T L,\\ &\qquad \left\|\mathbf{s}-\mathbf{s}_0\right\|_\infty \le \delta.\end{aligned} \tag{14}$$

Substituting (13) into the objective function of problem (14), and after some mathematical deduction, the problem (14) can be transformed into

$$\begin{aligned}&\max_{\mathbf{s}} \min_{n_1\in\mathcal{F},n_2\in\mathcal{J}} \mathbf{s}^H\mathbf{V}^H\left(f_t^{n_1},\phi_t^{n_2}\right)\mathbf{R}_{\mathrm{cn}}^{-1}\left(\mathbf{s}^{(i-1)}\right)\mathbf{V}\left(f_t^{n_1},\theta_t^{n_2}\right)\mathbf{s},\\ &\text{s.t.}\quad |\mathbf{s}(n)| = 1/\sqrt{N_T L},\ n=1,\cdots,N_T L,\\ &\qquad \left\|\mathbf{s}-\mathbf{s}_0\right\|_\infty \le \delta.\end{aligned} \tag{15}$$

Problem (15) is a nonconvex maximin problem, and it is difficult to find the optimal waveform in the polynomial time. A computationally efficient algorithm is derived to solve this problem. By introducing an auxiliary variable t, the maximin problem (15) can be transformed as

$$\begin{aligned}&\min_{\mathbf{s},t} -t,\\ &(1),\quad \mathbf{s}^H\mathbf{Q}^{n_1,n_2}\left(\mathbf{s}^{(i-1)}\right)\mathbf{s} \ge t,\ n_1\in\mathcal{F},\ n_2\in\mathcal{J},\\ &\text{s.t. } (2),\quad |\mathbf{s}(n)| = \frac{1}{\sqrt{N_T L}},\ n=1,\cdots,N_T L,\\ &(3),\quad \left\|\mathbf{s}-\mathbf{s}_0\right\|_\infty \le \delta.\end{aligned} \tag{16}$$

where

$$\mathbf{Q}^{n_1,n_2}\left(\mathbf{s}^{(i-1)}\right) = \mathbf{V}^H\left(f_t^{n_1},\phi_t^{n_2}\right)\mathbf{R}_{\mathrm{cn}}^{-1}\left(\mathbf{s}^{(i-1)}\right)\mathbf{V}\left(f_t^{n_1},\theta_t^{n_2}\right). \tag{17}$$

The objective function of problem (16) is convex, but the constraints are nonconvex. Then, the SCA technique is employed to deal with the nonconvex waveform constrains.

For the first constraint (1) in problem (16), since $\mathbf{Q}^{n_1,n_2}(\mathbf{s}^{(i-1)})$ is a semidefinite matrix, for any feasible solution $\mathbf{s}_f \in \mathbb{C}^{N_T L\times 1}$ of problem (14), the following inequality holds:

$$\left(\mathbf{s}-\mathbf{s}_f\right)^H\mathbf{Q}^{n_1,n_2}\left(\mathbf{s}^{(i-1)}\right)\left(\mathbf{s}-\mathbf{s}_f\right) \ge 0. \tag{18}$$

Expanding the left side of (18), we can obtain

$$\mathbf{s}^H\mathbf{Q}^{n_1,n_2}\left(\mathbf{s}^{(i-1)}\right)\mathbf{s} \ge 2\mathrm{Re}\left(\mathbf{s}^H\mathbf{Q}^{n_1,n_2}\left(\mathbf{s}^{(i-1)}\right)\mathbf{s}_f\right) - \mathbf{s}_f^H\mathbf{Q}^{n_1,n_2}\left(\mathbf{s}^{(i-1)}\right)\mathbf{s}_f. \tag{19}$$

Substituting inequality (19) into the first constraint of problem (16), we have

$$\begin{aligned}&\mathbf{s}_f^H\mathbf{Q}^{n_1,n_2}\left(\mathbf{s}^{(i-1)}\right)\mathbf{s}_f - 2\mathrm{Re}\left(\mathbf{s}^H\mathbf{Q}^{n_1,n_2}\left(\mathbf{s}^{(i-1)}\right)\mathbf{s}_f\right)\\ &\quad + t \le 0,\ n_1\in\mathcal{F},n_2\in\mathcal{J}.\end{aligned} \tag{20}$$

For the second constraint (2) in problem (16), it can be expressed as the intersection of $|\mathbf{s}(n)|^2 - 1/N_T L \le 0$ and $1/N_T L - |\mathbf{s}(n)|^2 \le 0$. The former is convex while the latter is nonconvex. Then, the first order condition of convex function is used to approximate the lower bound of $|\mathbf{s}(n)|^2$

$$\begin{aligned}|\mathbf{s}(n)|^2 &\ge \left|\mathbf{s}_f(n)\right|^2 + \mathrm{Re}\left\{\left(\frac{\partial|\mathbf{s}(n)|^2}{\partial\mathbf{s}(n)}|_{\mathbf{s}_f(n)}\right)^*\left(\mathbf{s}(n)-\mathbf{s}_f(n)\right)\right\}\\ &= \left|\mathbf{s}_f(n)\right|^2 + \mathrm{Re}\left\{2\mathbf{s}_f^*(n)\left(\mathbf{s}(n)-\mathbf{s}_f(n)\right)\right\}.\end{aligned} \tag{21}$$

Thus, the constraint $1/N_T L - |\mathbf{s}(n)|^2 \le 0$ can be approximately expressed as

$$\frac{1}{N_T L} - |\mathbf{s}(n)|^2 \le \frac{1}{N_T L} - \left|\mathbf{s}_f(n)\right|^2 - \mathrm{Re}\left\{2\mathbf{s}_f^*(n)\mathbf{s}(n) - 2\left|\mathbf{s}_f(n)\right|^2\right\} \le 0. \tag{22}$$

After some mathematical transformation, the second constraint (2) can be formulated as

$$\frac{1}{N_T L} - 2\mathrm{Re}\left\{\mathbf{s}_f^*(n)\mathbf{s}(n)\right\} + \left|\mathbf{s}_f(n)\right|^2 \le 0. \tag{23}$$

Expanding the third constraint (3) in problem (16), it can be expressed as $N_T L$ independent quadratic constraints, that is,

$$\left|\mathbf{s}(n)-\mathbf{s}_0(n)\right|^2 \le \delta^2,\quad n=1,\ldots,N_T L. \tag{24}$$

Therefore, by replacing the nonconvex constraints of problem (16) with convex approximate representations (20), (23), and (24), the convex approximate representation of problem (16) can be obtained

$$\begin{aligned}
&\min_{\mathbf{s},t} -t,\\
&\mathbf{s}_f^H \mathbf{Q}^{n_1,n_2}\left(\mathbf{s}^{(i-1)}\right)\mathbf{s}_f - 2\mathrm{Re}\left(\mathbf{s}^H \mathbf{Q}^{n_1,n_2}\left(\mathbf{s}^{(i-1)}\right)\mathbf{s}_f\right) + t \le 0, \quad n_1 \in \mathscr{I}, n_2 \in \mathscr{J},\\
&|\mathbf{s}(n)|^2 - \frac{1}{N_T L} \le 0, \quad \forall n,\\
&\text{s.t.}\\
&\frac{1}{N_T L} - 2\mathrm{Re}\left\{\mathbf{s}_f^*(n)\mathbf{s}(n)\right\} + \left|\mathbf{s}_f(n)\right|^2 \le 0, \quad \forall n,\\
&\left|\mathbf{s}(n) - \mathbf{s}_0(n)\right|^2 \le \delta^2, \quad \forall n.
\end{aligned} \tag{25}$$

However, since there is only one intersection of $|\mathbf{s}(n)|^2 - 1/N_T L \le 0$ and $1/N_T L - 2\mathrm{Re}\{\mathbf{s}_f^*(n)\mathbf{s}(n)\} + |\mathbf{s}_f(n)|^2 \le 0$, problem (25) has only a single feasible solution. Inspired by the iterative optimization algorithm and FPP algorithm [26–28], a nonnegative auxiliary variable was introduced to the third constraint of problem (25) and $\|\mathbf{u}\|_1$ is added to the objective function at the same time. At the ith iteration, problem (25) could be transformed into

$$\begin{aligned}
&\min_{\mathbf{s},t,\mathbf{u}} -t + \rho\|\mathbf{u}\|_1 + \kappa\left\|\mathbf{s} - \mathbf{s}^{(i-1)}\right\|^2\\
&\left(\mathbf{s}^{(i-1)}\right)^H \mathbf{Q}^{n_1,n_2}\left(\mathbf{s}^{(i-1)}\right)\mathbf{s}^{(i-1)} - 2\mathrm{Re}\left(\mathbf{s}^H \mathbf{Q}^{n_1,n_2}\left(\mathbf{s}^{(i-1)}\right)\mathbf{s}^{(i-1)}\right) + t \le 0, \quad n_1 \in \mathscr{I}, n_2 \in \mathscr{J},\\
&|\mathbf{s}(n)|^2 - \frac{1}{N_T L} \le 0, \ \forall n,\\
&\text{s.t.}\ \frac{1}{N_T L} - 2\mathrm{Re}\left\{\left(\mathbf{s}^{(i-1)}(n)\right)^* \mathbf{s}(n)\right\} + \left|\mathbf{s}^{(i-1)}(n)\right|^2 - \mathbf{u}(n) \le 0, \ \forall n,\\
&\left|\mathbf{s}(n) - \mathbf{s}_0(n)\right|^2 \le \delta^2, \ \forall n,\\
&\mathbf{u}(n) \ge 0, \ \forall n,\\
&t \ge t^{(i-1)},
\end{aligned} \tag{26}$$

where ρ and κ represent the positive penalty parameters. Supposing $(\mathbf{s}^{(i)}, t^{(i)})$ is the solution of the problem (26) at the ith iteration, and then the solution of the original problem (15) (or problem (16)) can be obtained by solving the optimization problem iteratively. It is worth noting that the norm $\|\mathbf{s} - \mathbf{s}^{(i-1)}\|^2$ is added to the objective function to ensure that a unique specific solution can be obtained when the problem (26) converges. The constraint $t \ge t^{(i-1)}$ is added to ensure that the algorithm obtains increasing solutions during the iteration. The question (26) belongs to the quadratically constrained quadratic programming (QCQP) problem, and it can be solved by transforming into second-order cone programming (SOCP). The interior point method (convex optimization tool kit [29]) is applied to obtain the optimal solution, whose computational complexity is $\mathcal{O}((N_T L)^3)$. The whole solution of transmit waveform is completed within the framework of the FPP-SCA algorithm, so it is called the transmit waveform optimization algorithm based on FPP-SCA.

4.3. Joint Design Method for Airborne MIMO Radar Based on FPP-SCA. The proposed joint design method based on FPP-SCA to solve problem (11) is summarized in Algorithm 1. The main computational complexity of the proposed method is dependent on the number of iterations and the computational complexity per iteration. In each iteration, the optimization of $\mathbf{w}_{n_1,n_2} \in \mathscr{W}$ for fixed $\mathbf{s}$ involves $\mathcal{O}((LMN_R)^3)$ complexity. The optimization of $\mathbf{s}$ for a given $\mathbf{w}_{n_1,n_2} \in \mathscr{W}$ has a complexity of $\mathcal{O}((N_T L)^3)$. The robust joint design method based on SDP and randomization (SDP-R) [30] can also address the problem (11), whose optimal waveform is obtained by interior point method involving $\mathcal{O}((N_T L)^{4.5})$ complexity. It is seen that the computational

complexity of the proposed joint design method is lower than that based on SDP-R.

Remark 1. The objective function $\overline{\mathrm{SCNR}}(\mathbf{s}^{(i)}, \mathbf{w}_{n_1,n_2}^{(i)})$ obtained by the joint design method based on FPP-SCA monotonically increases and converges to a specific value.

It is seen from (26) that the optimized value satisfies $t^{(i)} \geq t^{(i-1)}$. Thus, we have

$$\begin{aligned}\overline{\mathrm{SCNR}}\left(\mathbf{s}^{(i-1)}, \mathbf{w}_{n_1,n_2}^{(i-1)}\right) &= \min_{n_1\in\mathcal{I},n_2\in\mathcal{J}} \left(\mathbf{s}^{(i-1)}\right)^H \mathbf{V}^H\left(f_t^{n_1}, \phi_t^{n_2}\right)\boldsymbol{\Phi}_{\mathrm{cn}}^{-1}\left(\mathbf{s}^{(i-1)}\right)\mathbf{V}\left(f_t^{n_1}, \theta_t^{n_2}\right)\mathbf{s}^{(i-1)} \\ &\leq \min_{n_1\in\mathcal{I},n_2\in\mathcal{J}} \left(\mathbf{s}^{(i)}\right)^H \mathbf{V}^H\left(f_t^{n_1}, \phi_t^{n_2}\right)\boldsymbol{\Phi}_{\mathrm{cn}}^{-1}\left(\mathbf{s}^{(i-1)}\right)\mathbf{V}\left(f_t^{n_1}, \theta_t^{n_2}\right)\mathbf{s}^{(i)} \\ &= \overline{\mathrm{SCNR}}\left(\mathbf{s}^{(i)}, \mathbf{w}_{n_1,n_2}^{(i-1)}\right).\end{aligned} \tag{27}$$

5. Simulation Results

In this section, simulation results are implemented to validate the effectiveness of the proposed FPP-SCA based joint design method. The simulation scenario is set as follows: consider an airborne collocated MIMO radar with the transmit antenna and receive antenna being ULA, the number of transmit array is $N_T = 4$, the number of receive array is $N_R = 4$, the interelement spacing of the transmit antenna and receive antenna is $d_T = d_R = \lambda/2$, the pulse number within the coherent processing interval is $M = 4$, the PRF is $f_r = 2000$, and the sampling number of single pulse is $L = 8$. The platform altitude is 8000 m and the flight speed is $V_p = 140$ m/s. We consider the clutter of five range bin ($P = 2$) is received, the number of clutter patches of a single range bin is $N_c = 181$, and the clutter power is $\sigma_{c,p,k}^2 = R_0/R_p, p = -P, \cdots, P, k = 1, \cdots, N_c$, where R_0 and R_p, respectively, represent the distance from the range under test and the pth range bin to the platform. The noise power is 0 dB. The real position of the target on the space-time two-dimensional plane is (0.2, -0.2), the target uncertainty set is $\Psi = [0.1, 0.3]$ and $\Omega = [-0.3, -0.1]$, and the uniform sampling step is 0.02. Then, the number of sampling points of normalized Doppler frequency and normalized spatial frequency are 11, thus forming 121 groups of normalized Doppler frequency-spatial frequency pairs, and 121 groups of receive filters are required to process the received signals. The SNR is 20 dB. The orthogonal linear frequency modulation waveform is used as the reference waveform, i.e,

$$\mathbf{S}_0(n_t, l) = \frac{\exp\{j2\pi n_t(l-1)/L\}\exp\{j\pi(l-1)^2/L\}}{\sqrt{N_T L}}, \tag{28}$$

where $n_t = 1, \cdots, N_T$, $l = 1, \cdots, L$, and $\mathbf{s}_0 = \mathrm{vec}(\mathbf{S}_0)$. The parameters of FPP-SCA are set as follows: $\rho = 1$, $\eta = 10^{-4}$, and $\kappa = 10^{-5}$. The comparison algorithm is the robust joint design method based on SDP-R [30]. The iteration termination condition of SDP-R is 10^{-4} and the number of random trials of SDP-R is 1000. The simulation experiment platform is notebook (I7–9750U CPU and 32 GB RAM) Matlab 2016b.

Figure 3 shows the worst-case output SCNR versus the number of iterations. The similarity parameters are $\gamma = 0.4$, $\gamma = 1$, and $\gamma = 2$, respectively, where $\gamma = \delta\sqrt{N_T L}$. As can be seen from Figure 3, the worst-case output SCNR obtained by both FPP-SCA and SDP-R gradually increases with the increase of iterations. In addition, it is seen that all the worst-SCNR curves obtained by the proposed FPP-SCA remain unchanged when the number of iterations is greater than 5. This shows that the proposed algorithm is convergent. When the similarity parameter increases, the worst-case output SCNR of FPP-SCA and SDP-R also increases. It is worth noting that, when $\gamma = 0.4$, 1, and 2, the $\gamma = 0.4$ worst output SCNR obtained by the proposed FPP-SCA is significantly better than that obtained by SDP-R. For example, FPP-SCA is about 5.27 dB higher than SDP-R when $\gamma = 2$.

Table 1 provides the iteration number and runtime comparison of FPP-SCA and SDP-R, where $\gamma = 0.4$,1, and 2. As can be seen from Table 1, the total runtime of SDP-R is apparently larger than FPP-SCA for all γ. In addition, when $\gamma = 0.4$, 1, and 2, the running time change of FPP-SCA and SDP-R in a single iteration is relatively small. In particular, the running time of FPP-SCA and SDP-R in a single iteration is the largest when $\gamma = 0.4$ while the smallest when $\gamma = 1$. For fixed γ, the running time of a single iteration of FPP-SCA is significantly smaller than SDP-R. In fact, SDP-R method involves the solution of two SDP problems, and we can obtain from [30] that the computational complexity is $\mathcal{O}((LMN_R)^{4.5})$ and $\mathcal{O}((LN_T)^{4.5})$, respectively. Thus, the total computational complexity of the SDP-R method is $\mathcal{O}(\widetilde{I}((LMN_R)^{4.5} + t(LN_T)^{4.5}))$, where $\widetilde{I}$ denotes the number of iterations. Contrarily, the total computational complexity of FPP-SCA is $\mathcal{O}(\widetilde{I}((LMN_R)^3 + t(LN_T)^3))$, which is much smaller than that of SDP-R. In addition, the more constraints exist, the longer the running time of the SDP-R algorithm. For example, 121 groups of receive filters are set in this paper, and the number of constraints including receive filters is 121. Thus, the computational load is much heavy, which leads to a much longer running time required for a single iteration.

Figure 4 depicts the worst-case output SCNR versus the target uncertainty value, where the target normalized Doppler frequency error and the target spatial frequency error both increase from 0 to 0.2. In addition, the FPP-SCA-ROB represents "robust design," where the worst-case output SCNR is obtained by the proposed FPP-SCA iterative

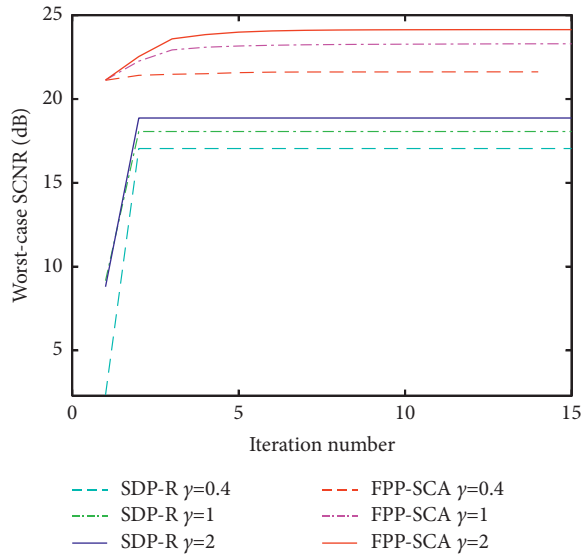

Figure 3: Worst-case output SCNR versus the iteration number.

Input: $\mathbf{V}(f_t^{n_1}, \phi_t^{n_2}), n_1 \in \mathcal{I}, n_2 \in \mathcal{J}$, $\mathbf{R}_{cn}(\mathbf{s})$, $\mathbf{w}_{n_1,n_2}^{(0)} \in \mathcal{W}$, $\mathbf{s}^{(0)}$, η
Output: The optimal solution to problem (11) $(\mathbf{s}^*, \mathbf{w}_{n_1,n_2}^* \in \mathcal{W})$.
Iteration:
Step 1: $i = 1$.
Step 2: Calculate $\mathbf{R}_{cn}(\mathbf{s}^{(i-1)})$ with (9) and $\mathbf{s}^{(i-1)}$, compute $\mathbf{w}_{n_1,n_2}^{(i)} \in \mathcal{W}$ with (13).
Step 3: Obtain the optimal waveform $\mathbf{s}^{(i)}$ by solving problem (26) with FPP-SCA algorithm.
Step 4: If $|\overline{\mathrm{SCNR}}(\mathbf{s}^{(i)}, t\mathbf{w}_{n_1,n_2}^{(i)}) - \overline{\mathrm{SCNR}}(\mathbf{s}^{(i-1)}, t\mathbf{w}_{n_1,n_2}^{(i-1)})| \le \eta$, stop the iteration, otherwise, go step 2.
Step 5: Output $\mathbf{s}^* = \mathbf{s}^{(i)}$ and $\mathbf{w}_{n_1,n_2}^* = \mathbf{w}_{n_1,n_2}^{(i)}$.

Algorithm 1: Joint design method based on FPP-SCA to solve (11).

Table 1: Iteration number and runtime comparison of different algorithm.

Algorithm	Total runtime (s)	Iteration number	Average runtime (s)
SDP-R ($\gamma = 0.4$)	494.82	3	164.94
SDP-R ($\gamma = 1$)	430.83	3	143.61
SDP-R ($\gamma = 2$)	438.81	3	146.27
FPP-SCA ($\gamma = 0.4$)	27.72	14	1.98
FPP-SCA ($\gamma = 1$)	31.96	17	1.88
FPP-SCA ($\gamma = 2$)	28.65	15	1.91

algorithm (where the number of receive filters is set as 121), while FPP-SCA-NROB denotes the "nonrobust design," where the output SCNR is obtained by the presumed target position (where the number of receive filters is set as 1). We can see that the output SCNR curves obtained by FPP-SCA-ROB and FPP-SCA-NROB all utilize the FPP-SCA iterative algorithm, where the difference between them lies in the number of receive filter bank. The more the number of receive filters, the stronger the robustness of the algorithm. The FPP-SCA-NROB is not robust against the target uncertainty value since the number of filter banks is set as 1. As can be seen from Figure 4, the worst-case output SCNR of FPP-SCA-NROB is a little better than FPP-SCA-ROB when the target uncertainty value is small. The reason is that more degree of freedom of the system is utilized to deal with the target uncertainty. It is seen that the worst-case output SCNR of FPP-SCA-ROB is higher than that of FPP-SCA-NROB when the target uncertainty value is larger than 0.08. Furthermore, the larger the value of target uncertainty value is, the more worst-case output SCNR of FPP-SCA-NROB decreases, while FPP-SCA-ROB decreases slowly. The simulation results demonstrate that the proposed FPP-SCA-ROB is robust to the target uncertainty parameters.

Figure 5 shows the worst-case output SCNR versus the target position, where the target normalized Doppler frequency ranges from 0 to 0.4, the target normalized spatial frequency ranges from −0.4 to 0, and the real position of the target is (0.2, −0.2). As can be seen from Figure 5, when the target is near the actual target location, the worst-case output SCNR of FPP-SCA-NROB is superior to that of FPP-SCA-ROB. However, when the target is far from the real location, the worst-case output SCNR of FPP-SCA-NROB is

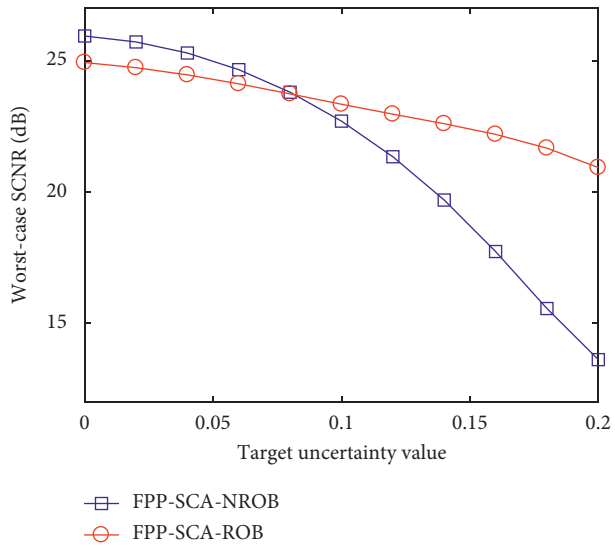

Figure 4: Worst-case output SCNR versus the target uncertainty value.

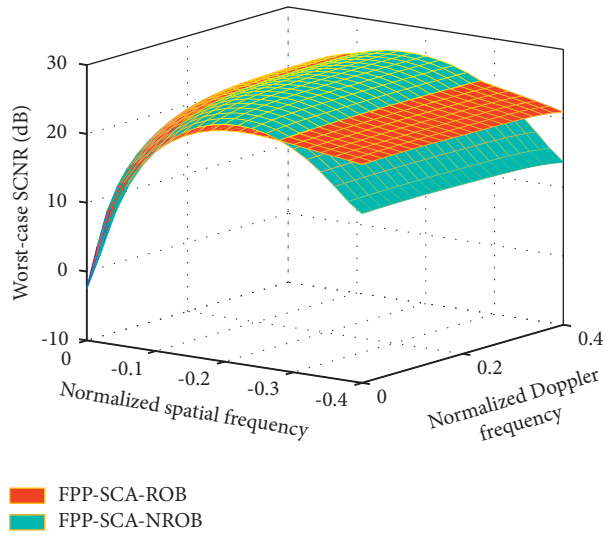

Figure 5: Worst-case output SCNR versus the target position.

significantly reduced, while the worst-case output SCNR of FPP-SCA-ROB remains relatively high value. This is consistent with the conclusion obtained in Figure 4. In addition, it can be observed from Figure 5 that when the target position tends to (0, 0), the worst-case output SCNR of both FPP-SCA-NROB and FPP-SCA-ROB decreases dramatically. The reason is that the point (0, 0) is the location of clutter, and the worst-case output SCNR forms a deep notch near the clutter ridge.

6. Conclusion

In order to improve the target detection performance of airborne MIMO radar when the target parameters have errors, a joint design method for transmit-receive of airborne MIMO radar based on FPP-SCA iteration is proposed in this paper. By designing a set of receive filters in the region where the target might appear, we can solve the SCNR degradation caused by the uncertain target parameters. Considering the constant-modulus constraint and similarity constraint of the transmit waveform, an FPP-SCA algorithm was designed to obtain the optimal waveform. Simulation results show that: (1) compared with the traditional joint design method based on SDP and randomization, the proposed method avoids the use of randomization to find the optimal waveform. In addition, we observe that for different similarity parameters γ, apparent worst-case output SCNR improvement is obtained by the proposed method with relatively small computational load. (2) The achieved worst-case SCNR becomes worse when the inaccuracy on the target parameters increases. Nevertheless, adopting more receive filters can provide a better robustness against these uncertainties than only one receive filter.

However, it should be mentioned that the number of receive filters is large in this work. In fact, the larger the number of receive filters, the greater the computational burden of the algorithm. The interval model, ball model,

ellipsoidal model, and norm model are good choice to describe the target uncertain parameters [31]. Besides, the spectral constraint on the transmit waveform is considered to ensure the spectrum coexistence with other communication systems [32–34]. Thus, all these directions are pursued in the future research.

Data Availability

The data used to support the findings of this study are available from the corresponding author upon request.

Conflicts of Interest

The authors declare that there are no conflicts of interest regarding the publication of this paper.

Acknowledgments

This work was supported in part by the National Natural Science Foundation of China under Grants 61901511, 62001510, and 62001479, and in part by the Anhui Provincial Natural Science Foundation under Grant 2108085QF257, and in part by the Research Program of National University of Defense Technology under Grants ZK19-10, ZK19-28 and ZK20-33.

References

[1] J. Ward, "Space-time adaptive processing for airborne radar," Technical report 1015, MIT Lincoln Laboratory, Lexington, MA, USA, 1994.

[2] R. Klemm, *Principles of Space-Time Adaptive Processing*, IET, London, UK, 3rd edition, 2006.

[3] W. L. Melvin, "Space-time adaptive radar performance in heterogeneous clutter," *IEEE Transactions on Aerospace and Electronic Systems*, vol. 36, no. 2, pp. 621–633, 2000.

[4] L. Lan, J. Xu, G. Liao, Y. Zhang, F. Fioranelli, and H. C. So, "Suppression of mainbeam deceptive jammer with FDA-MIMO radar," *IEEE Transactions on Vehicular Technology*, vol. 69, no. 10, Article ID 11598, 2020.

[5] J. Li and P. Stoica, "MIMO radar with colocated antennas," *IEEE Signal Processing Magazine*, vol. 24, no. 5, pp. 106–114, 2007.

[6] I. Bekkerman and J. Tabrikian, "Target detection and localization using MIMO radars and sonars," *IEEE Transactions on Signal Processing*, vol. 54, no. 10, pp. 3873–3883, 2006.

[7] J. Li and P. Stoica, *MIMO Radar Signal Processing*, John Wiley & Sons, incorporated, Hoboken, NJ, USA, 2009.

[8] H. Godrich, A. M. Haimovich, and R. S. Blum, "Target localization accuracy gain in MIMO radar-based systems," *IEEE Transactions on Information Theory*, vol. 56, no. 6, pp. 2783–2803, 2010.

[9] S. D. Blunt and E. L. Mokole, "Overview of radar waveform diversity," *IEEE Aerospace and Electronic Systems Magazine*, vol. 31, no. 11, pp. 2–42, 2016.

[10] J. Shi, Z. Yang, and Y. Liu, "On parameter identifiability of diversity-smoothing-based MIMO radar," *IEEE Transactions on Aerospace and Electronic Systems*, vol. 58, no. 3, pp. 1660–1675, 2022.

[11] S. Haykin, "Cognitive radar: A way of the future," *IEEE Signal Processing Magazine*, vol. 23, no. 1, pp. 30–40, 2006.

[12] B. Tang and J. Tang, "Joint design of transmit waveforms and receive filters for MIMO radar space-time adaptive processing," *IEEE Transactions on Signal Processing*, vol. 64, no. 18, pp. 4707–4722, 2016.

[13] P. Setlur and M. Rangaswamy, "Waveform design for radar STAP in signal dependent interference," *IEEE Transactions on Signal Processing*, vol. 64, no. 1, pp. 19–34, 2016.

[14] S. M. O'Rourke, P. Setlur, M. Rangaswamy, and A. L. Swindlehurst, "Relaxed biquadratic optimization for joint filter-signal design in signal-dependent STAP," *IEEE Transactions on Signal Processing*, vol. 66, no. 5, pp. 1300–1315, 2018.

[15] S. M. O'Rourk, P. Setlur, M. Rangaswamy, and A. L. Swindlehurst, "Quadratic semidefinite programming for waveform-constrained joint filter-signal design in STAP," *IEEE Transactions on Signal Processing*, vol. 68, pp. 1744–1759, 2020.

[16] S. Shi, Z. He, and Z. Wang, "Joint design of transmitting waveforms and receiving filter for MIMO-STAP airborne radar," *Circuits, Systems, and Signal Processing*, vol. 39, no. 3, pp. 1489–1508, 2020.

[17] J. Li, G. Liao, Y. Huang, and A. Nehorai, "Manifold optimization for joint design of MIMO-STAP radars," *IEEE Signal Processing Letters*, vol. 27, pp. 1969–1973, 2020.

[18] J. Li, G. Liao, Y. Huang, Z. Zhang, and A. Nehorai, "Riemannian geometric optimization methods for joint design of transmit sequence and receive filter on MIMO radar," *IEEE Transactions on Signal Processing*, vol. 68, pp. 5602–5616, 2020.

[19] Z. Li, Y. Mao, Q. Zhou, J. Shi, and B. Li, "Joint design of transmit beamforming and receive filter for transmit subaperturing MIMO STAP radar," *Multidimensional Systems and Signal Processing*, vol. 33, no. 1, pp. 143–165, 2022.

[20] H. Wang, G. Liao, J. Li, and H. Lv, "Waveform optimization for MIMO-STAP to improve the detection performance," *Signal Processing*, vol. 91, no. 11, pp. 2690–2696, 2011.

[21] B. Tang, J. Li, Y. Zhang, and J. Tang, "Design of MIMO radar waveform covariance matrix for Clutter and Jamming suppression based on space time adaptive processing," *Signal Processing*, vol. 121, pp. 60–69, 2016.

[22] Y. Wang, W. Li, Q. Sun, and G. Huang, "Robust joint design of transmit waveform and receive filter for MIMO radar space-time adaptive processing with signal-dependent interferences," *IET Radar, Sonar & Navigation*, vol. 11, no. 8, pp. 1321–1332, 2017.

[23] Q. Zhou, Z. Li, J. Shi, and Y. Mao, "Robust cognitive transmit waveform and receive filter design for airborne MIMO radar in signal-dependent clutter environment," *Digital Signal Processing*, vol. 101, pp. 1–15, 2020.

[24] Z. Li, B. Tang, J. Shi, and Q. Zhou, "Maximin joint design of transmit waveform and receive filter bank for MIMO-STAP radar under target uncertainties," *IEEE Signal Processing Letters*, vol. 29, pp. 179–183, 2022.

[25] Z. Li, J. Shi, W. Liu, J. Pan, and B. Li, "Robust joint design of transmit waveform and receive filter for MIMO-STAP radar under target and clutter uncertainties," *IEEE Transactions on Vehicular Technology*, vol. 71, no. 2, pp. 1156–1171, 2022.

[26] O. Mehanna, K. Huang, B. Gopalakrishnan, A. Konar, and N. D. Sidiropoulos, "Feasible point pursuit and successive approximation of non-convex QCQPs," *IEEE Signal Processing Letters*, vol. 22, no. 7, pp. 804–808, 2015.

[27] S. Imani and S. A. Ghorashi, "Sequential quasi-convex-based algorithm for waveform design in colocated multiple-input

multiple-output radars," *IET Signal Processing*, vol. 10, no. 3, pp. 309–317, 2016.

[28] X. Yu, K. Alhujaili, G. Cui, and V. Monga, "MIMO radar waveform design in the presence of multiple targets and practical constraints," *IEEE Transactions on Signal Processing*, vol. 68, pp. 1974–1989, 2020.

[29] M. Grant and S. Boyd, "Cvx package," 2012, http://www.cvxr.com/cvx.r.

[30] S. M. Karbasi, A. Aubry, A. De Maio, and M. H. Bastani, "Robust transmit code and receive filter design for extended targets in clutter," *IEEE Transactions on Signal Processing*, vol. 63, no. 8, pp. 1965–1976, 2015.

[31] Y. Xu, X. Zhao, and Y.-C. Liang, "Robust power control and beamforming in cognitive radio networks: A survey," *IEEE Communications Surveys & Tutorials*, vol. 17, no. 4, pp. 1834–1857, 2015.

[32] Z. Cheng, B. Liao, Z. He, Y. Li, and J. Li, "Spectrally compatible waveform design for MIMO radar in the presence of multiple targets," *IEEE Transactions on Signal Processing*, vol. 66, no. 13, pp. 3543–3555, 2018.

[33] A. Aubry, A. De Maio, M. A. Govoni, and L. Martino, "On the design of multi-spectrally constrained constant modulus radar signals," *IEEE Transactions on Signal Processing*, vol. 68, pp. 2231–2243, 2020.

[34] J. Yang, A. Aubry, A. De Maio, X. Yu, and G. Cui, "Multi-spectrally constrained transceiver design against signal-dependent interference," *IEEE Transactions on Signal Processing*, vol. 70, pp. 1320–1332, 2022.